

---

# Graph Neural Networks Do Not Always Oversmooth

---

Bastian Epping<sup>1</sup>, Alexandre René<sup>1</sup>, Moritz Helias<sup>2,3</sup>, Michael T. Schaub<sup>1</sup>

<sup>1</sup>RWTH Aachen University, Aachen, Germany

<sup>2</sup>Department of Physics, RWTH Aachen University, Aachen, Germany

<sup>3</sup>Institute for Advanced Simulation (IAS-6), Computational and Systems Neuroscience,  
Jülich Research Centre, Jülich, Germany

epping@cs.rwth-aachen.de, rene@cs.rwth-aachen.de,  
m.helias@fz-juelich.de, schaub@cs.rwth-aachen.de

## Abstract

Graph neural networks (GNNs) have emerged as powerful tools for processing relational data in applications. However, GNNs suffer from the problem of oversmoothing, the property that the features of all nodes exponentially converge to the same vector over layers, prohibiting the design of deep GNNs. In this work we study oversmoothing in graph convolutional networks (GCNs) by using their Gaussian process (GP) equivalence in the limit of infinitely many hidden features. By generalizing methods from conventional deep neural networks (DNNs), we can describe the distribution of features at the output layer of deep GCNs in terms of a GP: as expected, we find that typical parameter choices from the literature lead to oversmoothing. The theory, however, allows us to identify a new, non-oversmoothing phase: if the initial weights of the network have sufficiently large variance, GCNs *do not* oversmooth, and node features remain informative even at large depth. We demonstrate the validity of this prediction in finite-size GCNs by training a linear classifier on their output. Moreover, using the linearization of the GCN GP, we generalize the concept of propagation depth of information from DNNs to GCNs. This propagation depth diverges at the transition between the oversmoothing and non-oversmoothing phase. We test the predictions of our approach and find good agreement with finite-size GCNs. Initializing GCNs near the transition to the non-oversmoothing phase, we obtain networks which are both deep and expressive.

## 1 Introduction

Graph neural networks (GNNs) reach state of the art performance in diverse application domains with relational data that can be represented on a graph, transferring the success of machine learning to data on graphs [42, 11, 21, 7]. Despite their good performance, GNNs come with the limitation of *oversmoothing*, a phenomenon where node features converge to the same state exponentially fast for increasing depth [32, 40, 27, 2]. Consequently, only shallow networks are used in practice [17, 1]. In contrast, it is known that the depth (i.e. the number of layers) is key to the success of deep neural networks (DNNs) [29, 30]. While for conventional DNNs shallow networks are proven to be highly expressive [6], in practice deep networks are much easier to train and are thus the commonly used architectures [33]. Furthermore, in most GNN architectures each layer only exchanges information between neighboring nodes. Deep GNNs are therefore necessary to exchange information between nodes that are far apart in the graph [9]. In this study, we investigate oversmoothing in graph convolutional networks (GCNs) [17].

To study the effect of depth, we consider the propagation of features through the network: given some input  $x_\alpha^{(0)}$ , each intermediate layer  $l$  produces features  $x_\alpha^{(l)}$  which are fed to the next layer. We

follow the same approach that has successfully been employed in previous work to design trainable DNNs [34]: consider two nearly identical inputs  $\mathbf{x}_\alpha^{(0)}$  and  $\mathbf{x}_\beta^{(0)}$  and ask whether the intermediate features  $\mathbf{x}_\alpha^{(l)}$  and  $\mathbf{x}_\beta^{(l)}$  become more or less similar as a function of depth  $l$ . In the former case, the inputs may eventually become indistinguishable. In the latter case, the inputs become less similar over layers: the distance between them increases over layers [29, 34] until eventually it is bounded by the non-linearities of the network. The distance then typically converges to a fixed value determined by the network architecture, independent of the inputs.

One can therefore identify two phases: One says that a network is *regular* if two inputs eventually converge to the same value as function of  $l$ ; conversely, one says that a network is *chaotic* if two inputs remain distinct for all depths [22]. Neither phase is ideal for training deep networks since in both cases all the information from the inputs is eventually lost; the typical depth at which this happens is called the *information propagation depth*. However, this propagation depth diverges at the transition between the two phases, allowing information – in principle – to propagate infinitely deep into the network. While these results are calculated in the limit of infinitely many features in each hidden layer, the information propagation depth has been found to be a good indicator of how deep a network can be trained [34]. A usual approach for conventional DNNs is thus to initialize them at the transition to chaos. Indeed, Schoenholz et al. [34] were able to use this approach to train fully-connected, feedforward networks with hundreds of layers. Similar methods have recently been adapted to the study of transformers, successfully predicting the best hyperparameters for training [5].

In this work we address the oversmoothing problem of GCNs by extending the framework described above in the limit of infinite feature dimensions from DNNs to GCNs: here the two different inputs  $\mathbf{x}_\alpha^{(0)}$  and  $\mathbf{x}_\beta^{(0)}$  correspond to the input features on two nodes, labeled  $\alpha$  and  $\beta$ . The mixing of information across different nodes implies that output features on node  $\alpha$  depend on input features on node  $\beta$  and vice versa. Thus it is not possible to look at the distance of  $\mathbf{x}_\alpha^{(l)}$  and  $\mathbf{x}_\beta^{(l)}$  independently for each pair  $\alpha$  and  $\beta$  as in the DNN case. Rather, one has to solve for the distance between each distinct pair of nodes in the graph simultaneously: the one dimensional problem for DNNs thus becomes a multidimensional problem for GCNs. However, by linearizing the multidimensional GCN dynamics, we can generalize the notion of information propagation depth to GCNs: instead of being a single value, we find that a given GCN architecture comes with a set of potentially different information propagation depths, each corresponding to one eigendirection of the linearized dynamics of the system.

This approach allows us to extend the concept of a regular and a chaotic phase to GCNs: in the regular phase, which describes most of the GCNs studied in the current literature, distances between node features shrink over layers and exponentially attain the same value. We therefore call this the oversmoothing phase. On the other hand, if one increases the variance of the weights at initialization, it is possible to transition into the chaotic phase. In this phase, distances between node features converge to a fixed but finite distance at infinite depth. The convergence point is fully determined by the underlying graph structure and the hyperparameters of the GCN and may differ for different pairs of nodes. GCNs initialized in this phase thus do not suffer from oversmoothing. We find that the convergence point is informative about the topology of the underlying graph and may be used for node classification with GCNs of more than 1,000 layers. Near the transition point, GCNs at large depth offer a trade-off between feature information and information contained in the neighborhood relation of the graph. We test the predictions of this theory and find good agreement in comparison to finite-size GCNs applied to the contextual stochastic block model [8]. Our approach applies to graphs with arbitrary topologies, depths, and nonlinearities.

## 2 Related Work

Oversmoothing is a well-known challenge within the GNN literature [19, 32]. On the theoretical side, rigorous techniques have been used to prove that oversmoothing is inevitable. The authors in [27] show that GCNs with the ReLU non-linearity exponentially lose expressive power and only carry information of the node degree in the infinite layer limit. These results have been extended in [2] to handle non-linearities different from ReLU. Also graph attention networks have been proven

to oversmooth inevitably [40]. These proofs, however, make assumptions on the weight matrices which, as we will show, exclude networks in the chaotic, non-oversmoothing phase.

On the applied side, a variety of heuristics have been developed to mitigate oversmoothing [44, 4, 3, 20, 36, 14]. E.g., the authors in [44] introduce a normalization layer which can be added to a variety of deep GNNs to make them trainable. Another approach is to introduce residual connections and identity mappings, directly feeding the input to layers deep in the network [4, 41]. Other studies suggest to train GNNs to a limited number of layers to obtain the optimal amount of smoothing [16, 41]. The recent review [15] proposes a unified view to order existing heuristics and guide further research. While these heuristics improve performance at large depths, they also add to the complexity of the model and impose design choices. Our approach, on the other hand, explains why increasing the weight variance at initialization is sufficient to prevent oversmoothing.

### 3 Background

#### 3.1 Network architecture

In this paper we study a standard graph convolutional network (GCN) architecture [17] with an input feature matrix  $\mathbf{X}^{(0)} \in \mathbb{R}^{N \times d_0}$ , where  $N$  is the number of nodes in the graph and  $d_0$  the number of input features. Bold symbols throughout represent vector or matrix quantities in feature space. The structure of the graph is represented by a shift operator  $A \in \mathbb{R}^{N \times N}$ . We write the features of the network’s  $l$ -th layer as  $\mathbf{X}^{(l)} \in \mathbb{R}^{N \times d_l}$ ; they are computed recursively as

$$\mathbf{X}^{(l)} = \phi(A\mathbf{X}^{(l-1)}\mathbf{W}^{(l)\top} + \mathbf{1}\mathbf{b}^{(l)\top}), \quad (1)$$

with  $\phi$  an elementwise nonlinear activation function,  $\mathbf{b}^{(l)}$  an optional bias term, weight matrices  $\mathbf{W}^{(l)} \in \mathbb{R}^{d_l \times d_{l-1}}$ , and  $\mathbf{1} \in \mathbb{R}^N$  a vector of all ones. We note that many GNN architectures studied in the literature are unbiased, which can be recovered by setting  $\mathbf{b}^{(l)}$  to zero. We use a noisy linear readout, so that the output of the network is given by

$$Y = A\mathbf{X}^{(L)}\mathbf{W}^{(L+1)\top} + \mathbf{1}\mathbf{b}^{(L+1)\top} + \varepsilon, \quad (2)$$

with  $\varepsilon \in \mathbb{R}^N$  a vector of independent Gaussian random variables:  $\varepsilon_\alpha \stackrel{\text{i.i.d.}}{\sim} \mathcal{N}(0, \sigma_{ro}^2)$ . We set  $d_{L+1} = 1$  so that the GCN output at each node is scalar; the architecture, however, can easily be extended to multi-dimensional outputs [17].

For the following it will be useful to consider the activity of individual nodes. To avoid ambiguity in the indexing, we use lower Greek indices for nodes and upper Latin indices for layers. We thus rewrite (1) as

$$\mathbf{x}_\alpha^{(l)} = \phi(\mathbf{h}_\alpha^{(l)}), \quad (3)$$

$$\mathbf{h}_\alpha^{(l)} = \sum_\beta A_{\alpha\beta} \mathbf{W}^{(l)} \mathbf{x}_\beta^{(l-1)} + \mathbf{b}^{(l)}, \quad (4)$$

$$y_\alpha = \mathbf{h}_\alpha^{(L+1)} + \varepsilon_\alpha, \quad (5)$$

where  $\mathbf{x}_\alpha^{(l)} \in \mathbb{R}^{d_l}$  is the feature vector of node  $\alpha$  in layer  $l$  and  $y_\alpha \in \mathbb{R}$  the network output for node  $\alpha$ . The values  $\mathbf{h}_\alpha^{(l)} \in \mathbb{R}^{d_l}$  are linear functions of the features  $\mathbf{x}_\beta^{(l-1)}$  and represent the input to the activation functions; we therefore refer to them as preactivations. The nonlinearity  $\phi(x)$  is applied elementwise to the preactivations  $\mathbf{h}_\alpha^{(l)}$ . While we leave  $\phi(x)$  general for the development of the theory, we will use  $\phi(x) = \text{erf}(\frac{\sqrt{\pi}}{2}x)$  in our experiments in Section 4. The scaling factor in the erf is chosen such that  $\frac{\partial \phi}{\partial x}(0) = 1$ . We use independent and identical Gaussian priors for all weight matrices and biases,  $W_{ij}^{(l)} \stackrel{\text{i.i.d.}}{\sim} \mathcal{N}(0, \frac{\sigma_w^2}{d_l})$  and  $b_i^{(l)} \stackrel{\text{i.i.d.}}{\sim} \mathcal{N}(0, \sigma_b^2)$  with  $W_{ij}^{(l)}$  and  $b_i^{(l)}$  being the matrix or vector entries of  $\mathbf{W}^{(l)}$  and  $\mathbf{b}^{(l)}$ , respectively. As a shift operator, we choose

$$A = \mathbb{I} - \frac{g}{d_{\max}}(D - A), \quad (6)$$

where  $\mathcal{A}$  is the adjacency matrix,  $\mathbb{I}$  the identity in  $\mathbb{R}^{N \times N}$ ,  $D_{\alpha\beta} = \delta_{\alpha\beta} \sum_{\gamma} \mathcal{A}_{\alpha\gamma}$  is the degree matrix and  $d_{\max}$  is the maximal degree. The parameter  $g \in (0, 1)$  allows us to weigh the off-diagonal elements compared to the diagonal ones. By construction the shift operator is column stochastic, which means that it has constant sums over columns  $\sum_{\beta} A_{\alpha\beta} = \text{const.}$ . We will make use of this property in our analysis in Section 4.2. The generalization to non-stochastic shift operators is addressed in the discussion.

### 3.2 Gaussian process equivalence of GCNs

In a classic machine learning setting, such as classification, one draws random initial values for all parameters and subsequently trains the parameters by optimizing the weights and biases to minimize a loss function. This learned parameter set is then used to classify unlabeled inputs. In this paper we take a Bayesian point of view in which the network parameters are random variables, inducing a probability distribution over outputs which becomes Gaussian in the limit of infinitely many features. Thus infinitely wide neural networks are equivalent to Gaussian processes (GPs) [24, 38, 31]. In the study of DNNs this is a standard approach, yielding results which empirically hold also for finite-size networks trained with gradient descent [34].

In previous work [25, 13, 26] it has been shown that also the GCN architecture described in Section 3.1 is equivalent to a GP in the limit of infinite feature space dimensions,  $d_l \rightarrow \infty$  for all hidden layers  $l = 1, \dots, L$ , while input and readout layer still have tunable, finitely many features. In the GP description, all features are Gaussian random variables with zero mean and identical prior variance in each feature dimension. The description of the GCN thus reduces to a multivariate normal,

$$H^{(l)} \sim \mathcal{N}(0, K^{(l)}), \quad (7)$$

where  $H^{(l)}$  is the vector of hidden node features of layer  $l$ ,  $H^{(l)} = (h_0^{(l)}, h_1^{(l)}, \dots, h_N^{(l)})^\top$  under the prior distribution of weights and biases. The covariance matrices  $K^{(l)} \in \mathbb{R}^{N \times N}$  are determined recursively: knowing that the  $h_\alpha^{(l)}$  follow a zero-mean Gaussian with covariance  $\langle h_\delta^{(l)} h_\gamma^{(l)} \rangle = K_{\delta\gamma}^{(l)}$ , we define

$$C_{\gamma\delta}^{(l)} = \left\langle \phi\left(h_\gamma^{(l)}\right) \phi\left(h_\delta^{(l)}\right) \right\rangle_{h_\gamma^{(l)}, h_\delta^{(l)}}. \quad (8)$$

For simplicity we use  $\phi(x) = \text{erf}\left(\frac{\sqrt{\pi}}{2}x\right)$  for which Equation (8) can be evaluated analytically; see Appendix B for details. It follows from (3) that

$$K_{\alpha\beta}^{(l+1)} = \sigma_b^2 + \sigma_w^2 \sum_{\gamma, \delta} A_{\alpha\gamma} A_{\beta\delta} C_{\gamma\delta}^{(l)}, \quad (9)$$

as shown in [25, 26].

In a semi-supervised node classification setting, we split the underlying graph into  $N^{\text{test}}$  unlabeled test nodes and  $N^{\text{train}}$  labeled training nodes ( $N^{\text{test}} + N^{\text{train}} = N$ ); we correspondingly split the output random variable  $Y$  into  $Y_\star \in \mathbb{R}^{N^{\text{test}}}$  and  $Y_D \in \mathbb{R}^{N^{\text{train}}}$ . Features on the test nodes are predicted by conditioning on the values of the training nodes:  $p(Y_\star = y_\star \mid Y_D = y_D)$ . This leads to the following posterior for the unobserved labels (see [31, 18] for details):

$$Y_\star \sim \mathcal{N}(m^{\text{GP}}, K^{\text{GP}}), \quad (10)$$

$$m^{\text{GP}} = K_{\star D}^{(L+1)} (K_{DD}^{(L+1)} + \mathbb{I} \sigma_{r_o}^2)^{-1} Y_D, \quad (11)$$

$$K^{\text{GP}} = K_{\star\star}^{(L+1)} - K_{\star D}^{(L+1)} (K_{DD}^{(L+1)} + \mathbb{I} \sigma_{r_o}^2)^{-1} (K_{\star D}^{(L+1)})^\top. \quad (12)$$

Here the  $\star$  and  $D$  indices represent test and training data, respectively, i.e.  $K_{DD} \in \mathbb{R}^{N^{\text{train}} \times N^{\text{train}}}$  is the covariance matrix of outputs of all training nodes and  $K_{\star D} \in \mathbb{R}^{N^{\text{test}} \times N^{\text{train}}}$  is the covariance between test data and training data. Finally,  $\mathbb{I}$  is here the identity in  $\mathbb{R}^{N^{\text{train}} \times N^{\text{train}}}$ .

### 3.3 Feature distance

To measure and quantify how much a given GCN instance oversmooths we use the squared Euclidean distance between pairs of nodes, and normalize by the number of node features  $d_l$  so that the

measure stays finite in the GP limit  $d_l \rightarrow \infty$ . This allows us to quantitatively test the predictions of our approach on the node-resolved distances of features. To summarize the amount of oversmoothing across the GCN, we also define the measure  $\mu(X)$  as the average squared Euclidean distance across all pairs of nodes:

$$d(\mathbf{x}_\alpha, \mathbf{x}_\beta) = \frac{1}{d_l} \|\mathbf{x}_\alpha - \mathbf{x}_\beta\|_2^2 = C'_{\alpha\alpha} + C'_{\beta\beta} - 2C'_{\alpha\beta}, \quad (13)$$

$$\mu(\mathbf{X}) = \frac{1}{2N(N-1)} \sum_{\alpha=1}^N \sum_{\beta=\alpha+1}^N d(\mathbf{x}_\alpha, \mathbf{x}_\beta). \quad (14)$$

Here  $C'_{\alpha\beta} = \frac{\mathbf{x}_\alpha \cdot \mathbf{x}_\beta}{d_l}$  is the normalized scalar product. We use the notation  $C'_{\alpha\beta}$  to avoid confusion with the expectation value  $C_{\alpha\beta}$  defined in the GCN GP (8). In the infinite feature dimensions limit, the quantities  $C'_{\alpha\beta}$  in Equation (14) converge to the GCN GP quantities  $C_{\alpha\beta}$  defined by (8). In the following sections we will therefore use the  $C_{\alpha\beta}$  as predictions for the  $C'_{\alpha\beta}$  of finite-size GCNs. The normalization for  $d(\mathbf{x}_\alpha, \mathbf{x}_\beta)$  and  $\mu(\mathbf{X})$  can be interpreted as an average (squared) feature distance, independent of the size of the graph and the number of feature dimensions.

## 4 Results

### 4.1 Propagation depths

We are interested in analyzing GCNs at large depth. We a priori assume that at infinite depth the GCN converges to an equilibrium in which covariances are static over layers  $K_{\alpha\beta}^{(l)} \xrightarrow{l \rightarrow \infty} K^{\text{eq}}$ , irrespective of whether the GCN is in the oversmoothing or the chaotic phase. A posteriori we show that this assumption indeed holds. Since the fixed point  $K^{\text{eq}}$  is independent of the input, a GCN at equilibrium cannot use information from the input to make predictions (although, as we will see, in the non-oversmoothing phase it can still use the graph structure). In the following we analyze the equilibrium covariance  $K^{\text{eq}}$  to which GCNs with different  $\sigma_w^2$ ,  $\sigma_b^2$  and  $A$  converge to, how they behave near this equilibrium, and at which rate it is approached.

Close to equilibrium, the covariance matrix  $K^{(l)}$  can be written as a perturbation around  $K_{\alpha\beta}^{\text{eq}}$ :

$$K_{\alpha\beta}^{(l)} = K_{\alpha\beta}^{\text{eq}} + \Delta_{\alpha\beta}^{(l)}. \quad (15)$$

Under the assumption that the perturbation  $\Delta_{\alpha\beta}^{(l)}$  is small, we can linearize the GCN GP

$$\Delta_{\alpha\beta}^{(l+1)} = \sum_{\gamma\delta} H_{\alpha\beta,\gamma\delta} \Delta_{\gamma\delta}^{(l)} + \mathcal{O}((\Delta^{(l)})^2), \quad (16)$$

$$H_{\alpha\beta,\gamma\delta} = \sigma_w^2 \sum_{\theta\phi} \frac{1}{2} (1 + \delta_{\gamma,\delta}) A_{\alpha\theta} A_{\beta\phi} \frac{\partial C_{\theta\phi}}{\partial K_{\gamma\delta}} [K^{\text{eq}}], \quad (17)$$

where we use square brackets to denote the point around which we linearize.

A conceptually similar linearization has been done in [34] for DNNs. In the DNN case, different inputs to the networks—which correspond to input features on different nodes here—can be treated separately, leading to decoupling of Equation (16). The shift operator in the GCN dynamics, in contrast, couples features on neighboring nodes – the matrix  $H_{\alpha\beta,\gamma\delta}$  is in general not diagonal.

We can still achieve a decoupling by interpreting Equation (16) as a matrix multiplication, if  $\alpha\beta$  and  $\gamma\delta$  are understood as double indices, and by finding the eigendirections of the matrix  $H \in \mathbb{R}^{N^2 \times N^2}$ . Taking the right eigenvectors  $V_{\alpha\beta}^{(i)}$  as basis vectors, we can decompose the covariance matrix  $\Delta_{\alpha\beta}^{(l)} = \sum_i \Delta_i^{(l)} V_{\alpha\beta}^{(i)}$  and thus obtain the overlaps  $\Delta_i^{(l)}$  which evolve independently over layers. If the fixed point  $K^{\text{eq}}$  is attractive, all eigenvalues have absolute values smaller than one:  $|\lambda_i| < 1$ . This allows us to define the propagation depth  $\xi_i := -\frac{1}{\ln|\lambda_i|}$  for each eigendirection, very similar to the DNN case [34]. In this form, the linear update equation (16) simplifies to

$$\Delta_i^{(l+d)} = \lambda_i^d \Delta_i^{(l)} = \exp(-d/\xi_i) \Delta_i^{(l)}, \quad (18)$$

thus decoupling the system. For details on the linearization and some properties of the transition matrix  $H$  refer to Appendix A.

## 4.2 The non-oversmoothing phase of GCNs

In this section we establish the chaotic, non-oversmoothing phase of GCNs, and show that this phase can be reached by simple tuning of the weight variance  $\sigma_w^2$  at initialization. We start by noticing that a GCN is at a state of zero feature distance  $\mu(\mathbf{X}^{(l)}) = 0$ , if the covariance matrix has constant entries,  $K_{\alpha\beta}^{(l)} = k^{(l)}$ : Constant entries in  $K_{\alpha\beta}^{(l)}$  imply that all preactivations are the same,  $\mathbf{h}_\alpha^{(l)} = \mathbf{h}_\beta^{(l)}$ , which in turn implies  $C_{\alpha\beta}^{(l)} = c^{(l)}$  (by Equation (8)); the latter is equivalent to features being the same,  $\mathbf{x}_\alpha^{(l)} = \mathbf{x}_\beta^{(l)}$ . Due to our choice of the shift operator, the state of zero distance (and thus of  $K_{\alpha\beta}^{(l)} = k^{(l)}$ ) is a always fixed point. Assuming that  $C_{\alpha\beta}^{(l)} = c^{(l)}$ , we obtain

$$K_{\alpha\beta}^{(l+1)} = \sigma_b^2 + \sigma_w^2 \underbrace{\sum_{\gamma} A_{\alpha\gamma}}_{=1} \underbrace{\sum_{\delta} A_{\beta\delta}}_{=1} c^{(l)} = k^{(l+1)}. \quad (19)$$

In an overmoothing GCN, this fixed point is also attractive, meaning that also pairs of feature inputs  $\mathbf{x}_\alpha^{(0)}, \mathbf{x}_\beta^{(0)}$  which initially have non-zero distance  $d(\mathbf{x}_\alpha^{(0)}, \mathbf{x}_\beta^{(0)}) \neq 0$  (and thus  $\mu(\mathbf{X}^{(0)}) \neq 0$ ) eventually converge to the point of vanishing distance. The chaotic, non-oversmoothing phase of a GCN is determined by the condition that this point of constant covariance  $K_{\alpha\beta}^{(l)} = k^{(l)}$  becomes unstable. More formally, this can be written in terms of eigenvalues of the linearized dynamics as

$$\max\{|\lambda_i^p|\} \stackrel{?}{>} 1. \quad (20)$$

Here and in the following we will use the superscript p to denote that the linearization is done around the state of constant covariance across nodes in both the overmoothing and non-oversmoothing phase. The propagation depth  $\xi_i := -\frac{1}{\ln|\lambda_i|}$  diverges at the phase transition where one  $\lambda_i$  approaches 1. Intuitively speaking, Equation (20) asks whether a small perturbation from the zero distance case diminishes ( $\max\{|\lambda_i^p|\} < 1$ ), in which case the network dynamics is regular, or grows ( $\max\{|\lambda_i^p|\} > 1$ ), in which case the network is chaotic and thus does not oversmooth. The value of  $\max\{|\lambda_i^p|\}$  depends on the choices of  $A$ ,  $\sigma_w^2$  and  $\sigma_b^2$  (by the dependence of  $K^{\text{eq}}$  on  $\sigma_b^2$ ). In the following we will concentrate on tuning  $\sigma_w^2$  to reach the non-oversmoothing phase.

### 4.2.1 Complete graph

To illustrate the implications of the analysis described above, we first consider a particularly simple GCN on a complete graph; this allows us to calculate the condition for the transition to chaos analytically, and gain some insight into the interesting parameter regimes. Moreover, we use this pedagogical example to show that although the GP equivalence is only true in the limit of infinite hidden feature dimensions,  $d_l \rightarrow \infty$ , our results still describe finite-size GCNs well.

For a complete graph with adjacency matrix  $A_{\alpha\beta} = 1 - \delta_{\alpha\beta}$ , our choice of shift operator  $A$  in (6) has entries  $A_{\alpha\beta} = \frac{g}{N-1} + \delta_{\alpha\beta}(1 - \frac{Ng}{N-1})$ . This model is a worst-case scenario for overmoothing, since the adjacency matrix leads to inputs that are shared across all nodes of the network. We make the ansatz that the equilibrium covariance is of the form  $K_{\alpha\beta}^{\text{eq}} = K_c^{\text{eq}} + \delta_{\alpha\beta}(K_a^{\text{eq}} - K_c^{\text{eq}})$  due to symmetry which reduces the problem to only two variables. In this formulation we can use similar methods as in the DNN case [34] to determine the non-oversmoothing condition on the l.h.s in (20) (Details are given in Appendix C).

Figure 1 shows how a GCN on a complete graph can be engineered to be non-oversmoothing by simple tuning of the weight variance  $\sigma_w^2$ . Panel a) shows the feature distance  $\mu(\mathbf{X})$  in equilibrium as a heatmap dependent on the weight variance  $\sigma_w^2$  and the parameter  $g$  which determines the size of the off-diagonal elements of the shift operator  $A$  (6). The red line is the theoretical prediction for the transition to the non-oversmoothing phase as calculated in Appendix C. The distance  $\mu(\mathbf{X})$  increases from zero to finite values away from the transition into the non-oversmoothing phase. For larger values of  $g$ , the transition to chaos happens at larger values of  $\sigma_w^2$ : This makes sense intuitively, because smaller values of  $g$  increase smoothing, so higher values of  $\sigma_w^2$  are needed to counteract. The qualitative difference between the two phases is emphasized in panel b), where we depict  $\mu(\mathbf{X})$  in equilibrium close to zero as black and white else. Thus our formalism correctly predicts the transition to the non-oversmoothing phase, allowing us to control how strongly the

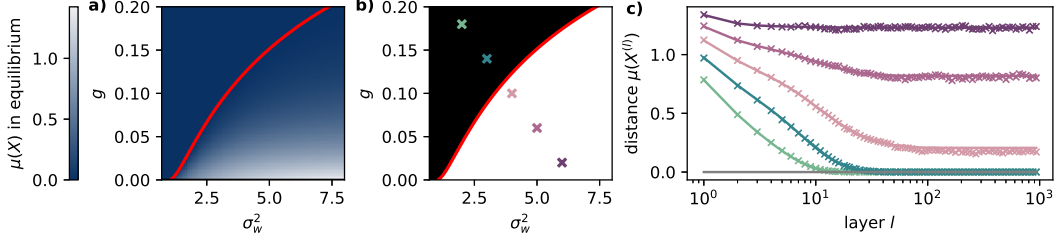


Figure 1: Simulations and GP prior of a GCN on a complete graph with  $N = 5$  nodes, shift operator  $A_{\alpha\beta} = \frac{g}{N-1} + \delta_{\alpha\beta}(1 - \frac{Ng}{N-1})$ , vanishing bias  $\sigma_b^2 = 0$  and  $\phi(x) = \text{erf}(\frac{\sqrt{\pi}}{2}x)$ . **a)** The phase diagram dependent on  $\sigma_w^2$  and  $g$ . The equilibrium feature distance  $\mu(\mathbf{X})$  obtained from computing the GCN GP prior for  $L = 4,000$  layers is shown as a heatmap, the red line is the theoretical prediction for the transition to the non-oversmoothing phase. **b)** Same as in a) but color coding shows whether  $\mu(\mathbf{X})$  is close to zero (black) or not (white) with precision  $10^{-5}$ . The red line again shows the theoretically predicted phase transition. **c)** Feature distance  $\mu(\mathbf{X}^{(l)})$  for a random input  $X_{\alpha i}^{(0)} \stackrel{\text{i.i.d.}}{\sim} \mathcal{N}(0, 1)$  as a function of layer  $l$  for  $(\sigma_w^2, g) = (2, 0.18)$ ,  $(3, 0.14)$  (green) and  $(\sigma_w^2, g) = (4, 0.1)$ ,  $(5, 0.06)$ ,  $(6, 0.02)$  (purple). The parameters are marked with color coded crosses in the phase diagram in panel b). Feature dimension of the hidden layers is  $d_l = 200$ , crosses show the mean of 50 network realizations, solid curves the theoretical predictions.

GCN oversmooths. Panel c) shows the evolution of feature distance (13) over layers for randomly generated input features for different values of  $\sigma_w^2$  and  $g$  in a finite-size GCN and compares it to the GP prediction. The network parameters are marked with crosses of matching colors in panel b). While the network converges to zero feature distance in the oversmoothing phase, it converges to finite values of  $\mu(\mathbf{X})$  in the chaotic, non-oversmoothing phase, meaning that in these cases the network does not oversmooth.

#### 4.2.2 General graphs

For general graphs, the transition to the non-oversmoothing phase given by Equation (20) can be determined numerically. As a proof of concept, we demonstrate this approach for the Contextual Stochastic Block Model (CSBM) [8], a common synthetic model which allows generating a graph with two communities and community-wise correlated features on the nodes. Pairs of nodes within the same community have higher probability of being connected and have feature vectors which are more strongly correlated, compared with pairs of nodes from different communities.

Given the underlying graph structure, we can construct the linear map  $H$  from Equation (16) and the analytical solution for  $C_{\theta\phi}$  in Appendix B. Finding the set of eigenvalues is then a standard task. We show the applicability of our formalism in Figure 2 by showing that GCNs degenerate to a zero distance state exactly when  $\sigma_w^2 < \sigma_{w,\text{crit}}^2$ . Panel a) shows the maximal eigenvalue of the linearized GCN GP dynamics around the zero distance state,  $\max\{\lambda^p\}$ , together with the maximum feature distance between any two pairs of nodes in the graph,  $\max_{(\alpha,\beta)}\{d(\mathbf{x}_\alpha, \mathbf{x}_\beta)\}$ . The maximum feature distance increases from zero at the point where the state  $K_{\alpha\beta}^{(l)} = k^{(l)}$  becomes unstable. This means that beyond this point, the GCN has feature vectors that differ across nodes and therefore does not oversmooth. This is explicitly shown in panels b) and c), where the equilibrium feature distance is plotted as a heatmap. At point A (panel b)), within the oversmoothing phase, all equilibrium feature distances are indeed zero, the network therefore converged to a state in which all features are the same. At point B (panel c)) on the other hand, pairs of nodes exist that have finite distance. Panel d) shows the feature distance averaged within the same community and across communities as a function of layers. While both converge to finite values, the averaged feature distance is larger for pairs of nodes across communities. The equilibrium state thus contains information about the graph topology. This aspect can also be observed in the block structure of the distance matrix in panel c). We thus showed that also on more general graphs the presented formalism predicts the transition point between the oversmoothing and the non-oversmoothing phase, corresponding to a transition between regular and chaotic behavior.

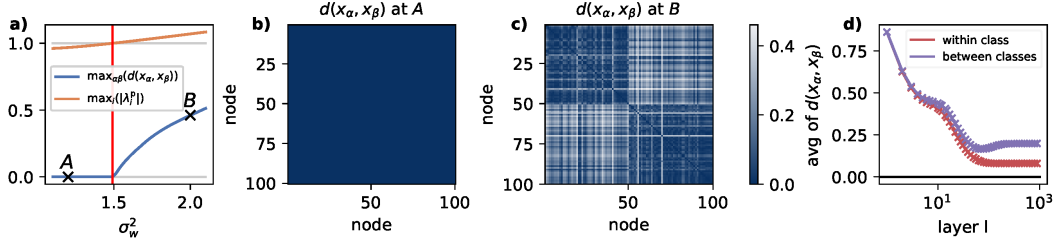


Figure 2: The non-oversmoothing phase in a contextual stochastic block model instance with parameters  $N = 100$ ,  $d = 5$ ,  $\lambda = 1$ . The shift operator is chosen according to (6) with  $g = 0.3$ , and  $\sigma_b^2 = 0$  and  $\phi(x) = \text{erf}(\frac{\sqrt{\pi}}{2}x)$ . **a)** The maximum feature distance between any pair of two nodes in equilibrium (blue) and the largest eigenvalue of the linearized GCN GP dynamics at the zero distance state as a function of weight variance  $\sigma_w^2$ . The red line marks the point where  $\max_i \{|\lambda_i^p|\} = 1$ . **b)** Heatmap of the equilibrium distance matrix with entries  $d_{\alpha\beta} = d(\mathbf{x}_\alpha, \mathbf{x}_\beta)$  (Equation (13)) at  $\sigma_w^2 = 1.3$ , marked as point *A* in panel a). Colorbar shared with the plot in c). **c)** Same as b) but at point *B* with  $\sigma_w^2 = 2.0$ . **d)** Features distances  $d_{\alpha\beta}^{(l)} = d(\mathbf{x}_\alpha^{(l)}, \mathbf{x}_\beta^{(l)})$  as a function of layers for random inputs  $X_{\alpha i}^{(0)} \stackrel{\text{i.i.d.}}{\sim} \mathcal{N}(0, 1)$  and a finite-size GCN with  $d_l = 200$ , averaged for distances for pairs of nodes within the same community (red) and across communities (purple).

We discuss how the assumptions on weight matrices in related theoretical work [2, 40] exclude networks in the chaotic phase in Appendix E, explaining why the non-oversmoothing phase has not been reported before.

### 4.3 Implications for performance

Lastly we want to investigate the implications of the non-oversmoothing phase on performance. We do this by applying the GCN GP as well as a finite-size GCN to the task of node classification in the CSBM model and measure their performance, shown in Figure (3). Panel a) shows the generalization error (mean squared error) averaged over multiple instances of CSBMs dependent on the weight variance  $\sigma_w^2$  and number of layers  $l$ . In the oversmoothing phase where most GCNs in the literature are initialized (see Appendix E), the generalization error increases significantly already after only a couple of layers. We observe the best performance near the transition to chaos where the GCN GP stays informative up to 100 layers. Panel b) shows the performance of the GCN GP as a function of  $\sigma_w^2$  for a fixed number of layers ( $L = 1, 4, 16, 64, 256, 1024$  from turquoise to dark blue). While the generalization error increases to one (being random chance) in the oversmoothing phase, GCN GPs in the chaotic phase stay informative even at more than a thousand layers. This can be explained by Figure 2: For such deep networks, the dynamics are very close to the equilibrium and thus no information of the input features  $\mathbf{X}^{(0)}$  is transferred to the output. The state, however, still contains information of the network topology from the adjacency matrix, leading to better than random chance performance. In panel c) we explicitly show the layer dependence of the generalization error for the GCN GP at the critical point ( $\sigma_w^2 = \sigma_{w,\text{crit}}^2$ ), in the oversmoothing ( $\sigma_w^2 = \sigma_{w,\text{crit}}^2 - 1$ ) and in the chaotic phase ( $\sigma_w^2 = \sigma_{w,\text{crit}}^2 + 1$ ). Again, we see a fast performance drop for oversmoothing networks, while in the chaotic phase and at the critical point the GCN GP obtain good performance also at large depths, whereby performance peaks at  $L \approx 15$  layers. Thus tuning the weight variance does not only prevent oversmoothing, but may also come with computational benefits by allowing additional layers.

In the study of deep networks, results obtained in the limit of infinite feature dimensions  $d_l \rightarrow \infty$  often are also applicable for finite-size networks [29, 34]. In panel d) we conduct a preliminary analysis for finite-size GCNs by measuring the performance of randomly initialized GCNs for which we only train the readout layer via gradient descent. Indeed, we observe similar behavior as for the GCN GP: Performance drops rapidly over layers in the oversmoothing phase, while performance stays high over many layers at the critical point and in the chaotic phase and peaks at  $L \approx 15$  layers.



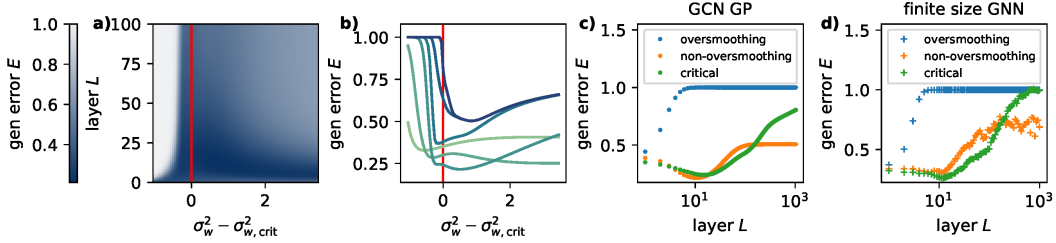


Figure 3: Generalization error (mean squared error) of the Gaussian process for a CSBM with parameters  $N = 20$ ,  $d = 5$ ,  $\lambda = 1$ ,  $\gamma = 1$  and  $\mu = 4$ . The shift operator is defined in (6) with  $g = 0.9$ , other parameters are  $\sigma_b^2 = 0$ ,  $\phi(x) = \text{erf}(\frac{\sqrt{\pi}}{2}x)$  and  $\sigma_{ro} = 0.01$ . In both panels we use  $N^{\text{train}} = 10$  training nodes and  $N^{\text{test}} = 10$  test nodes, five training nodes from each of the two communities. Labels are  $\pm 1$  for the two communities, respectively. For all panels, we show averages over 50 CSBM instances. **a)** Heatmap of the generalization error of the GCN GP dependent on number of layers  $L$  and weight variance  $\sigma_w^2$ . The red line shows the transition to the non-oversmoothing phase. **b)** Generalization error dependent on weight variance  $\sigma_w^2$  and  $L = 1, 4, 16, 64, 256, 1024$  from turquoise to dark blue. **c)** Generalization error dependent on the layer for the GCN GP at the critical line  $\sigma_w^2 = \sigma_{w,\text{crit}}^2$ , in the oversmoothing phase  $\sigma_w^2 = \sigma_{w,\text{crit}}^2 - 1$  and the non-oversmoothing phase  $\sigma_w^2 = \sigma_{w,\text{crit}}^2 + 1$ . **d)** Performance of randomly initialized finite-size GCNs with  $d_l = 200$  for  $l = 1, \dots, L$  where only the linear readout layer is trained with gradient descent (details in Appendix D) at the critical line  $\sigma_w^2 = \sigma_{w,\text{crit}}^2$ , in the oversmoothing phase  $\sigma_w^2 = \sigma_{w,\text{crit}}^2 - 1$  and the non-oversmoothing phase  $\sigma_w^2 = \sigma_{w,\text{crit}}^2 + 1$ .

## 5 Discussion

In this study we used the equivalence of GCNs and GPs to investigate oversmoothing, the property that features at different nodes converge over layers to the same feature vector in an exponential manner. By extending concepts such as the propagation depth and chaos from the study of conventional deep feedforward neural networks [34], we are able to derive a condition to avoid oversmoothing. This condition is phrased in terms of an eigenvalue problem of the linearized GCN GP dynamics around the state where all features are the same: This state is stable if all eigenvalues are smaller than one, thus the networks do not oversmooth. If one eigenvalue, however, is larger than one, the state where the features are the same on all nodes becomes unstable. While most GCNs studied in the literature are in the oversmoothing phase [2, 40], the non-oversmoothing phase can be reached by a simple tuning of the weight variance at initialization. An analogy can be drawn between the chaotic phase of DNNs and the non-oversmoothing phase of GCNs. Previous theoretical works have proven that oversmoothing is inevitable in some GNN architectures, among them GCNs; these works, however, make crucial assumptions on the weight matrices, constraining their variances to be in what we identify as the oversmoothing phase.

**Limitations.** The current analysis is based on the equivalence of GCNs and GPs which strictly holds only in the limit of infinite feature dimension. GCNs with large feature vectors ( $d_l = 200$ ) are well described by the theory, as shown in Section 4. For a small number of feature dimensions, however, we expect deviations from the asymptotic results. Throughout this work, we assumed a column-stochastic shift operator which made the equilibrium  $K^{\text{eq}}$  in the oversmoothing phase particularly simple. For other shift operators, we expect the equilibrium  $K^{\text{eq}}$  to look different in detail. Yet, we hypothesize that increasing the weight variance makes the equilibrium more informative of the graph topology, as in the stochastic shift operator case. The choice of nonlinearity is unrestricted, but in the general case numerical integration of (8) is needed.

To determine whether a given weight variance is in the non-oversmoothing phase, one calculates the eigenvalues of the linearized GCN GP dynamics which take the form of an  $N^2 \times N^2$  matrix (see Equation (16)), this has a run time of  $\mathcal{O}(N^6)$ . While this becomes computationally expensive for large graphs, the conceptual insights of the presented analysis remain. In practical applications with large graphs one may reduce the computational load by determining the transition point via computation of the GCN GP prior until it is close to equilibrium. This procedure has a runtime of  $\mathcal{O}(N^2 L^{\text{eq}})$  where  $L^{\text{eq}}$  is the number of layers after which the process is sufficiently close to

equilibrium. One might then do an interval search on the weight variance until the transition point is determined with sufficient accuracy.

**Outlook.** Formulating GCNs with the help of GPs can be considered the leading order in the number of feature space dimension  $d_l$  when approximating finite-size GCNs. Computing corrections for finite numbers of hidden feature dimensions would allow the characterization of feature learning in such networks, similar as in standard deep networks [23, 43, 35]. Moreover, the generalization of this formalism to more general shift operators and other GNN architectures [44, 4] are possible directions of future research.

### Acknowledgements

Funded by the European Union (ERC, HIGH-HOPeS, 101039827). Views and opinions expressed are however those of the author(s) only and do not necessarily reflect those of the European Union or the European Research Council Executive Agency. Neither the European Union nor the granting authority can be held responsible for them. We also acknowledge funding by the German Research Council (DFG) within the Collaborative Research Center “Sparsity and Singular Structures” (SfB 1481; Project A07).

### References

- [1] Uri Alon and Eran Yahav. On the Bottleneck of Graph Neural Networks and its Practical Implications, March 2021. arXiv:2006.05205 [cs, stat].
- [2] Chen Cai and Yusu Wang. A Note on Over-Smoothing for Graph Neural Networks, June 2020. arXiv:2006.13318 [cs, stat].
- [3] Deli Chen, Yankai Lin, Wei Li, Peng Li, Jie Zhou, and Xu Sun. Measuring and Relieving the Over-Smoothing Problem for Graph Neural Networks from the Topological View. *Proceedings of the AAAI Conference on Artificial Intelligence*, 34(04):3438–3445, April 2020. Number: 04.
- [4] Ming Chen, Zhewei Wei, Zengfeng Huang, Bolin Ding, and Yaliang Li. Simple and Deep Graph Convolutional Networks. In *Proceedings of the 37th International Conference on Machine Learning*, pages 1725–1735. PMLR, November 2020. ISSN: 2640-3498.
- [5] Aditya Cowsik, Tamra Nebabu, Xiao-Liang Qi, and Surya Ganguli. Geometric Dynamics of Signal Propagation Predict Trainability of Transformers, March 2024. arXiv:2403.02579 [cond-mat].
- [6] G. Cybenko. Approximation by superpositions of a sigmoidal function. *Mathematics of Control, Signals and Systems*, 2(4):303–314, December 1989.
- [7] Michaël Defferrard, Xavier Bresson, and Pierre Vandergheynst. Convolutional Neural Networks on Graphs with Fast Localized Spectral Filtering. In *Advances in Neural Information Processing Systems*, volume 29. Curran Associates, Inc., 2016.
- [8] Yash Deshpande, Subhabrata Sen, Andrea Montanari, and Elchanan Mossel. Contextual Stochastic Block Models. In *Advances in Neural Information Processing Systems*, volume 31. Curran Associates, Inc., 2018.
- [9] Vijay Prakash Dwivedi, Ladislav Rampásek, Michael Galkin, Ali Parviz, Guy Wolf, Anh Tuan Luu, and Dominique Beaini. Long Range Graph Benchmark. *Advances in Neural Information Processing Systems*, 35:22326–22340, December 2022.
- [10] Jean Ginibre. Statistical Ensembles of Complex, Quaternion, and Real Matrices. *Journal of Mathematical Physics*, 6(3):440–449, March 1965.
- [11] William L. Hamilton. *Graph Representation Learning*. Morgan & Claypool Publishers, September 2020.
- [12] Charles R. Harris, K. Jarrod Millman, Stéfan J. van der Walt, Ralf Gommers, Pauli Virtanen, David Cournapeau, Eric Wieser, Julian Taylor, Sebastian Berg, Nathaniel J. Smith, Robert Kern, Matti Picus, Stephan Hoyer, Marten H. van Kerkwijk, Matthew Brett, Allan Hal-dane, Jaime Fernández del Río, Mark Wiebe, Pearu Peterson, Pierre Gérard-Marchant, Kevin Sheppard, Tyler Reddy, Warren Weckesser, Hameer Abbasi, Christoph Gohlke, and Travis E. Oliphant. Array programming with NumPy. *Nature*, 585(7825):357–362, September 2020. Publisher: Nature Publishing Group.

- [13] Jilin Hu, Jianbing Shen, Bin Yang, and Ling Shao. Infinitely Wide Graph Convolutional Networks: Semi-supervised Learning via Gaussian Processes, February 2020. arXiv:2002.12168 [cs, stat].
- [14] Tianjin Huang, Tianlong Chen, Meng Fang, Vlado Menkovski, Jiaxu Zhao, Lu Yin, Yulong Pei, Decebal Constantin Mocanu, Zhangyang Wang, Mykola Pechenizkiy, and Shiwei Liu. You Can Have Better Graph Neural Networks by Not Training Weights at All: Finding Untrained GNNs Tickets, February 2024. arXiv:2211.15335 [cs].
- [15] Yufei Jin and Xingquan Zhu. ATNPA: A Unified View of Oversmoothing Alleviation in Graph Neural Networks, May 2024. arXiv:2405.01663 [cs].
- [16] Nicolas Keriven. Not too little, not too much: a theoretical analysis of graph (over)smoothing. *Advances in Neural Information Processing Systems*, 35:2268–2281, December 2022.
- [17] Thomas N. Kipf and Max Welling. Semi-Supervised Classification with Graph Convolutional Networks, February 2017. arXiv:1609.02907 [cs, stat].
- [18] Jaehoon Lee, Yasaman Bahri, Roman Novak, Samuel S. Schoenholz, Jeffrey Pennington, and Jascha Sohl-Dickstein. Deep Neural Networks as Gaussian Processes, March 2018. arXiv:1711.00165 [cs, stat].
- [19] Qimai Li, Zhichao Han, and Xiao-ming Wu. Deeper Insights Into Graph Convolutional Networks for Semi-Supervised Learning. *Proceedings of the AAAI Conference on Artificial Intelligence*, 32(1), April 2018. Number: 1.
- [20] Sitao Luan, Mingde Zhao, Xiao-Wen Chang, and Doina Precup. Training Matters: Unlocking Potentials of Deeper Graph Convolutional Neural Networks, October 2022. arXiv:2008.08838 [cs, stat].
- [21] Yao Ma and Jiliang Tang. *Deep Learning on Graphs*. Cambridge University Press, September 2021. Google-Books-ID: \_AVDEAAAQBAJ.
- [22] L. Molgedey, J. Schuchhardt, and H. G. Schuster. Suppressing chaos in neural networks by noise. *Physical Review Letters*, 69(26):3717–3719, December 1992. Publisher: American Physical Society.
- [23] Gadi Naveh and Zohar Ringel. A self consistent theory of Gaussian Processes captures feature learning effects in finite CNNs. In *Advances in Neural Information Processing Systems*, volume 34, pages 21352–21364. Curran Associates, Inc., 2021.
- [24] Radford M Neal. Priors for infinite networks (tech. rep. no. crg-tr-94-1). *University of Toronto*, 415, 1994.
- [25] Yin Cheng Ng, Nicolò Colombo, and Ricardo Silva. Bayesian Semi-supervised Learning with Graph Gaussian Processes. In *Advances in Neural Information Processing Systems*, volume 31. Curran Associates, Inc., 2018.
- [26] Zehao Niu, Mihai Anitescu, and Jie Chen. Graph Neural Network-Inspired Kernels for Gaussian Processes in Semi-Supervised Learning, February 2023. arXiv:2302.05828 [cs, stat].
- [27] Kenta Oono and Taiji Suzuki. Graph Neural Networks Exponentially Lose Expressive Power for Node Classification, January 2021. arXiv:1905.10947 [cs, stat].
- [28] Fabian Pedregosa, Gaël Varoquaux, Alexandre Gramfort, Vincent Michel, Bertrand Thirion, Olivier Grisel, Mathieu Blondel, Peter Prettenhofer, Ron Weiss, Vincent Dubourg, Jake Vanderplas, Alexandre Passos, David Cournapeau, Matthieu Brucher, Matthieu Perrot, and Édouard Duchesnay. Scikit-learn: Machine Learning in Python. *Journal of Machine Learning Research*, 12(85):2825–2830, 2011.
- [29] Ben Poole, Subhaneil Lahiri, Maithra Raghu, Jascha Sohl-Dickstein, and Surya Ganguli. Exponential expressivity in deep neural networks through transient chaos. In *Advances in Neural Information Processing Systems*, volume 29. Curran Associates, Inc., 2016.
- [30] Maithra Raghu, Ben Poole, Jon Kleinberg, Surya Ganguli, and Jascha Sohl-Dickstein. On the Expressive Power of Deep Neural Networks. In *Proceedings of the 34th International Conference on Machine Learning*, pages 2847–2854. PMLR, July 2017. ISSN: 2640-3498.
- [31] Carl Edward Rasmussen and Christopher K. I. Williams. *Gaussian processes for machine learning*. Adaptive computation and machine learning. MIT Press, Cambridge, Mass, 2006. OCLC: ocm61285753.

- [32] T. Konstantin Rusch, Michael M. Bronstein, and Siddhartha Mishra. A Survey on Oversmoothing in Graph Neural Networks, March 2023. arXiv:2303.10993 [cs].
- [33] Andrew M. Saxe, James L. McClelland, and Surya Ganguli. Exact solutions to the nonlinear dynamics of learning in deep linear neural networks, February 2014. arXiv:1312.6120 [cond-mat, q-bio, stat].
- [34] Samuel S. Schoenholz, Justin Gilmer, Surya Ganguli, and Jascha Sohl-Dickstein. Deep Information Propagation, April 2017. arXiv:1611.01232 [cs, stat].
- [35] Inbar Seroussi, Gadi Naveh, and Zohar Ringel. Separation of scales and a thermodynamic description of feature learning in some CNNs. *Nature Communications*, 14(1):908, February 2023. Number: 1 Publisher: Nature Publishing Group.
- [36] Yunchong Song, Chenghu Zhou, Xinbing Wang, and Zhouhan Lin. Ordered GNN: Ordering Message Passing to Deal with Heterophily and Over-smoothing, February 2023. arXiv:2302.01524 [cs].
- [37] Pauli Virtanen, Ralf Gommers, Travis E. Oliphant, Matt Haberland, Tyler Reddy, David Cournapeau, Evgeni Burovski, Pearu Peterson, Warren Weckesser, Jonathan Bright, Stéfan J. van der Walt, Matthew Brett, Joshua Wilson, K. Jarrod Millman, Nikolay Mayorov, Andrew R. J. Nelson, Eric Jones, Robert Kern, Eric Larson, C. J. Carey, İlhan Polat, Yu Feng, Eric W. Moore, Jake VanderPlas, Denis Laxalde, Josef Perktold, Robert Cimrman, Ian Henriksen, E. A. Quintero, Charles R. Harris, Anne M. Archibald, António H. Ribeiro, Fabian Pedregosa, and Paul van Mulbregt. SciPy 1.0: fundamental algorithms for scientific computing in Python. *Nature Methods*, 17(3):261–272, March 2020. Publisher: Nature Publishing Group.
- [38] Christopher Williams. Computing with Infinite Networks. In *Advances in Neural Information Processing Systems*, volume 9. MIT Press, 1996.
- [39] Christopher K. I. Williams. Computation with Infinite Neural Networks. *Neural Computation*, 10(5):1203–1216, July 1998.
- [40] Xinyi Wu, Amir Ajorlou, Zihui Wu, and Ali Jadbabaie. Demystifying Oversmoothing in Attention-Based Graph Neural Networks, October 2023. arXiv:2305.16102 [cs, stat].
- [41] Xinyi Wu, Zhengdao Chen, William Wang, and Ali Jadbabaie. A Non-Asymptotic Analysis of Oversmoothing in Graph Neural Networks, February 2023. arXiv:2212.10701 [cs, stat].
- [42] Zonghan Wu, Shirui Pan, Fengwen Chen, Guodong Long, Chengqi Zhang, and Philip S. Yu. A Comprehensive Survey on Graph Neural Networks. *IEEE Transactions on Neural Networks and Learning Systems*, 32(1):4–24, January 2021. Conference Name: IEEE Transactions on Neural Networks and Learning Systems.
- [43] Jacob A. Zavatone-Veth, William L. Tong, and Cengiz Pehlevan. Contrasting random and learned features in deep Bayesian linear regression. *Physical Review E*, 105(6):064118, June 2022. Publisher: American Physical Society.
- [44] Lingxiao Zhao and Leman Akoglu. PairNorm: Tackling Oversmoothing in GNNs, February 2020. arXiv:1909.12223 [cs, stat].

## A The linearized GP of GCNs

We start from the full GCN GP iterative map which we restate here for readability

$$K_{\alpha\beta}^{(l+1)} = T_{\alpha\beta}[K^{(l)}] = \sigma_b^2 + \sigma_w^2 \sum_{\gamma,\delta} A_{\alpha\gamma} A_{\beta\delta} \left\langle \phi\left(h_\gamma^{(l)}\right) \phi\left(h_\delta^{(l)}\right) \right\rangle_{h_\gamma^{(l)}, h_\delta^{(l)}} \quad (21)$$

where  $h_\gamma^{(l)}$  and  $h_\delta^{(l)}$  are drawn from a 0-mean Gaussian distribution with covariance  $\langle h_\gamma^{(l)} h_\delta^{(l)} \rangle = K_{\gamma\delta}^{(l)}$ . The full covariance matrix of layer  $l$  is denoted as  $K^{(l)}$ . Here, we differentiate between the iterative maps  $T_{\alpha\beta} : \mathbb{R}^{N \times N} \rightarrow \mathbb{R}$  of which there are  $N^2$ , one for each pair of nodes  $\alpha$  and  $\beta$ , and the entries of the covariance matrix in the layer  $l + 1$  being  $K_{\alpha\beta}^{(l+1)}$ . Notice that  $T_{\alpha\beta} = T_{\beta\alpha}$  due to the symmetry of the covariance matrix. In the maps  $T_{\alpha\beta}$ , the covariance matrix of the previous layer only shows up in the expectation value  $C_{\gamma\delta} = \left\langle \phi\left(h_\gamma^{(l)}\right) \phi\left(h_\delta^{(l)}\right) \right\rangle_{h_\gamma^{(l)}, h_\delta^{(l)}}$  such that the linearized

dynamics around a fixed point (being equilibrium  $K_{\alpha\beta}^{\text{fix}} = K_{\alpha\beta}^{\text{eq}}$  or zero distance state  $K_{\alpha\beta}^{\text{fix}} = k$ ) with  $K_{\alpha\beta}^{(l)} = K_{\alpha\beta}^{\text{fix}} + \Delta_{\alpha\beta}^{(l)}$  read

$$\begin{aligned}
K_{\alpha\beta}^{(l+1)} &= K_{\alpha\beta}^{\text{fix}} + \Delta_{\alpha\beta}^{(l+1)} = \underbrace{T_{\alpha\beta}[K^{\text{fix}}]}_{=K_{\alpha\beta}^{\text{fix}}} + \sum_{\gamma < \delta} \frac{\partial T_{\alpha\beta}}{\partial K_{\gamma\delta}} [K^{\text{fix}}] \Delta_{\gamma\delta}^{(l)} + \mathcal{O}((\Delta^{(l)})^2) \\
&= K_{\alpha\beta}^{\text{fix}} + \sum_{\gamma, \delta} \sigma_w^2 \sum_{\theta, \phi} \frac{1}{2} (1 + \delta_{\gamma, \delta}) A_{\alpha\theta} A_{\beta\phi} \underbrace{\frac{\partial C_{\theta\phi}}{\partial K_{\gamma\delta}} [K^{\text{fix}}] \Delta_{\gamma\delta}^{(l)}}_{\equiv H_{\alpha\beta, \gamma\delta}} + \mathcal{O}((\Delta^{(l)})^2),
\end{aligned} \tag{22}$$

where we restrict the sum in (22) to  $\gamma < \delta$  since  $K_{\gamma\delta}$  and  $K_{\delta\gamma}$  are the same quantity. From (22) follows

$$\Delta_{\alpha\beta}^{(l+1)} = \sum_{\gamma\delta} H_{\alpha\beta, \gamma\delta} \Delta_{\gamma\delta}^{(l)} + \mathcal{O}((\Delta^{(l)})^2) \tag{24}$$

which is Equation (16) in the main text. While  $H$  is not symmetric in general,  $H_{\alpha\beta, \gamma\delta} \neq H_{\gamma\delta, \alpha\beta}$ , it is symmetric in the first and second pair of covariance indices,  $H_{\alpha\beta, \gamma\delta} = H_{\beta\alpha, \gamma\delta}$  and  $H_{\alpha\beta, \gamma\delta} = H_{\alpha\beta, \delta\gamma}$  due to symmetry of the covariance matrices,  $K_{\alpha\beta} = K_{\beta\alpha}$ .

In the main text, we look for the right eigenvectors of  $H$  fulfilling

$$\lambda_i V_{\alpha\beta}^{(i)} = \sum_{\gamma\delta} H_{\alpha\beta, \gamma\delta} V_{\gamma\delta}^{(i)}. \tag{25}$$

These are for general non-symmetric matrices not orthogonal. In order to decompose  $\Delta^{(l)}$  to overlaps with the eigenvectors  $V_{\alpha\beta}^{(i)}$  we need to find the dual vectors  $U_{\alpha\beta}^{(i)}$  fulfilling

$$\sum_{\alpha\beta} U_{\alpha\beta}^{(i)} V_{\alpha\beta}^{(j)} = \delta_{ij} \tag{26}$$

from which we can define

$$\Delta_i^{(l)} = \sum_{\alpha\beta} U_{\alpha\beta}^{(i)} \Delta_{\alpha\beta}^{(l)} \tag{27}$$

such that

$$\Delta_{\alpha\beta}^{(l)} = \sum_i \Delta_i^{(l)} V_{\alpha\beta}^{(i)} \tag{28}$$

as stated in the main text.

## B Analytical solution for expectation values

To evaluate our theory, we need to compute expectation values given in the form of 8 which we restate here for readability

$$C_{\gamma\delta}^{(l)} = \left\langle \phi\left(h_\gamma^{(l)}\right) \phi\left(h_\delta^{(l)}\right) \right\rangle_{h_\gamma^{(l)}, h_\delta^{(l)}}, \tag{29}$$

where  $h_\gamma^{(l)}$  and  $h_\delta^{(l)}$  are zero mean random Gaussian variables with  $\langle h_\gamma^{(l)} h_\delta^{(l)} \rangle = K_{\gamma\delta}^{(l)}$ . This can be evaluated numerically for general nonlinearities  $\phi(x)$ . For simplicity, however, we choose  $\phi(x) = \text{erf}\left(\frac{\sqrt{\pi}}{2}x\right)$  in our experiments where the scaling factor in the erf is chosen such that  $\frac{\partial\phi}{\partial x}(0) = 1$ . In this case, the expectation value can be evaluated analytically to be

$$C_{\gamma\delta}^{(l)} = \frac{2}{\pi} \arcsin \left( \frac{\frac{\pi}{2} K_{\gamma\delta}^{(l)}}{\sqrt{1 + \frac{\pi}{2} K_{\gamma\gamma}^{(l)}} \sqrt{1 + \frac{\pi}{2} K_{\delta\delta}^{(l)}}} \right). \tag{30}$$

as shown in [39].

## C Investigation of the complete graph model

In this section we analytically investigate the complete graph model as defined in the main text. Specifically, we consider networks with the shift operator

$$A_{\alpha\beta} = \frac{g}{N-1} + \delta_{\alpha\beta}\left(1 - \frac{Ng}{N-1}\right) \quad (31)$$

and  $\phi = \text{erf}(\sqrt{\pi}x/2)$ . Due to the symmetry of the system we make the ansatz

$$K_{\alpha\beta}^{\text{eq}} = K_a^{\text{eq}} + \delta_{\alpha\beta}(K_c^{\text{eq}} - K_a^{\text{eq}}), \quad (32)$$

meaning that we assume constant variances  $K_a^{\text{eq}}$  across nodes and that all pairs of nodes have the same covariance  $K_c^{\text{eq}}$ , reducing the system to only two unknown variables. The equilibrium is a fixed point of the iterative map of the GCN GP. With the special choice of shift operator in (31) this becomes

$$K_a^{(l+1)} = \sigma_b^2 + g_a C_a^{(l)} + g_c C_c^{(l)} \quad (33)$$

and

$$K_c^{(l)} = \sigma_b^2 + h_a C_a^{(l)} + h_c C_c^{(l)} \quad (34)$$

with constants

$$g_a = \left(1 + \frac{g^2}{N-1}\right)\sigma_w^2 \quad (35)$$

$$g_c = 2\left(g + \frac{g^2(N-2)}{N-1}\right)\sigma_w^2 \quad (36)$$

$$h_a = 2\left(\frac{g}{N-1} + \frac{g^2(N-2)}{(N-1)^2}\right)\sigma_w^2 \quad (37)$$

$$h_c = \left(1 + \frac{g^2}{(N-1)^2} + 2\frac{g^2(N-2)(N-3)}{(N-1)^2} + 4\frac{g(N-2)}{(N-1)}\right)\sigma_w^2 \quad (38)$$

and

$$C_a^{(l)} = \langle \phi(h_\alpha^{(l)})\phi(h_\alpha^{(l)}) \rangle \quad (39)$$

$$C_c^{(l)} = \langle \phi(h_\alpha^{(l)})\phi(h_\beta^{(l)}) \rangle \quad \text{for } \alpha \neq \beta. \quad (40)$$

The preactivations are Gaussian distributed with zero mean and covariance  $\langle h_\alpha^{(l)} h_\beta^{(l)} \rangle = K_{\alpha\beta}^{(l)}$ . In the oversmoothing phase, we know that  $\mu(\mathbf{X}) = 0$  in equilibrium. We have seen in Section 4.2 that this corresponds to  $K_{\alpha\beta}^{\text{eq}} = k^{\text{eq}}$ , implying for our ansatz that  $K_c^{\text{eq}} = K_a^{\text{eq}}$ . We will find the transition to chaos by calculating where this state becomes unstable with regard to small perturbations. Specifically, we define  $c^{(l)} = \frac{K_c^{(l)}}{K_a^{(l)}}$  and look for the parameter point where

$$1 > \left. \frac{\partial c^{(l+1)}}{\partial c^{(l)}} \right|_{c^{(l)}=1}. \quad (41)$$

The authors in [34] used this approach to find the transition to chaos for DNNs. The correlation coefficient is

$$c^{(l+1)} = \frac{K_c^{(l+1)}}{K_a^{(l+1)}} = \frac{\sigma_b^2 + h_a C_a^{(l)} + h_c C_c^{(l)}}{\sigma_b^2 + g_a C_a^{(l)} + g_c C_c^{(l)}} \quad (42)$$

and Equation (41) thus becomes

$$\left. \frac{\partial c^{(l+1)}}{\partial c^{(l)}} \right|_{c^{(l)}=1} = \frac{h_c \frac{\partial C_c^{(l+1)}}{\partial c^{(l)}} K_a^{(l+1)} - g_c \frac{\partial C_c^{(l+1)}}{\partial c^{(l)}} K_c^{(l+1)}}{(K_a^{(l+1)})^2}. \quad (43)$$

Since we look at this equation at the perfectly correlated state  $c^{(l)} = 1$ , we know that  $K_a^{(l)} = K_c^{(l)}$  (implying that  $C_a^{(l)} = C_c^{(l)}$ ) and can determine  $K_a^{(l)}$  as the solution of the fixed point equation

$$K_a^{(l+1)} = \sigma_b^2 + (g_a + g_c)C_a^{(l)} \quad (44)$$

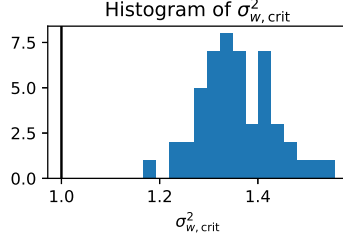


Figure 4: Histogram of  $\sigma_{w,\text{crit}}^2$  for the 50 CSBM instances used in the experiment of Figure 3. The point 1 is marked for comparison to related work.

to which the GCN GP dynamics reduce in the zero distance state (by using the fact that  $\sum_{\beta} A_{\alpha\beta} = 1$  an  $C_{\alpha\beta}^{(l)} = c^{(l)}$ ). Lastly, we can calculate

$$\frac{\partial C_c^{(l+1)}}{\partial c^{(l)}} \Big|_{c=1} = \frac{\partial}{\partial c^{(l)}} \left( \frac{2}{\pi} \arcsin \left( \frac{\frac{\pi}{2} K_a^{(l)} c^{(l)}}{1 + \frac{\pi}{2} K_a^{(l)}} \right) \right) \Big|_{c^{(l)}=1} \quad (45)$$

$$= \frac{2}{\pi} \frac{1}{\sqrt{1 - \left( \frac{\frac{\pi}{2} K_a^{(l)} c^{(l)}}{1 + \frac{\pi}{2} K_a^{(l)}} \right)^2}} \frac{K_a^{(l)}}{\frac{2}{\pi} + K_a^{(l)}} \Big|_{c^{(l)}=1} \quad (46)$$

$$= \frac{2}{\pi} \frac{1}{\sqrt{1 - \left( \frac{K_a^{(l)}}{\frac{2}{\pi} + K_a^{(l)}} \right)^2}} \frac{K_a^{(l)}}{\frac{2}{\pi} + K_a^{(l)}}, \quad (47)$$

where we used the known solution for the expectation value  $C_c$  for  $\phi(x) = \text{erf}(\sqrt{\pi}x/2)$  from Appendix B. Plugging this into Equation (43) lets us calculate  $\frac{\partial c^{(l+1)}}{\partial c^{(l)}} \Big|_{c^{(l)}=1}$  and thus determine the transition to the non-oversmoothing phase. This is plotted as a red line in Figure 1 panel a) and b).

## D Details of numerical experiments

To conduct our experiments we use NumPy [12], SciPy [37] (both available under a BSD-3-Clause License) and Scikit-learn (sklearn) [28] (available under a New BSD License). Computations were performed on CPUs, the requirements for the experiments are (approximately):

- Figure 1: 10mins on a single core laptop.
- Figure 2: 10h on a single node on an internal CPU cluster. Most of the computation time is needed for evaluating  $\max(\lambda_i^p)$  in panel a).
- Figure 3: 2h on a single core laptop. In panel d), the last layer of finite-size GCNs is trained with the standard settings from `sklearn.linear_model.SGDRegressor()`

## E Restriction of weight matrices in related work

In this section we will show histograms of critical weight variances  $\sigma_{w,\text{crit}}^2$  and discuss how the assumptions in [2] and [40] exclude networks in the non-oversmoothing phase. Our results thus stand in no conflict with the results of these works.

Here we want to argue that the assumptions on the weight matrices in related work constrains their architectures to the oversmoothing phase. We start with [40] in which the authors study graph attention networks (GATs). Although we study a standard GCN here, we hypothesize that increasing the weight variance at initialization likewise prevents oversmoothing in other architecture, such as the GAT in [40]. The critical assumption constraining them to the oversmoothing phase is their assumption A3, stating that  $\{ \|\prod_{l=0}^k |W^{(l)}| \|_{\max} \}_{k=0}^{\infty}$  is bounded where  $\|M\|_{\max} = \max_{i,j} |M_{i,j}|$ . For our setting of randomly drawn weight matrices  $W_{ij}^{(l)} \stackrel{\text{i.i.d.}}{\sim} \mathcal{N}(0, \frac{\sigma_w^2}{d_l})$  with  $W_{ij}^{(l)} \in \mathbb{R}^{N \times N}$ , this

restricts us to values  $\sigma_w^2 \leq 1$ . This can be seen by using the circular law from random matrix theory [10]: It is known that the eigenvalues of a matrix with i.i.d. random Gaussian entries of the form above have eigenvalues uniformly distributed in a circle around 0 in the complex plane with radius  $\sqrt{\sigma_w^2}$  in the limit  $d_l \rightarrow \infty$ . Thus, the maximal real part of any eigenvalue of this matrix is  $\sqrt{\sigma_w^2}$ . Thus we can estimate  $\|\prod_{l=0}^k |W^{(l)}|\|_{\max} \leq c(\sqrt{\sigma_w^2})^k$  with a constant  $c$ . To enter the non-oversmoothing phase, we need  $\sigma_w^2 > 1$ . In this case, the latter expression diverges for  $k \rightarrow \infty$ , thus being excluded by the proof in [40]. Indeed, for the CSBMs we investigated in this work, all critical weight variances  $\sigma_{w,\text{crit}}^2$  are larger than 1 as shown in Figure 4. Also in our model of the complete graph and the CSBM investigated in Section 4.2.2 all  $\sigma_{w,\text{crit}}^2$  are larger than 1, compare Figure 1 and Figure 2.

In [2] which is based on [27] the authors study GCNs, however with a different shift operator than we have in our work. In both of these works the authors state that the GCN exponentially loses expressive power if  $s\bar{\lambda} < 1$  with  $\bar{\lambda}$  being the maximal singular value/eigenvalue of the shift operator and  $s$  being the maximal singular value of all weight matrices. Again, the maximal singular value is limited (dependent on  $\bar{\lambda}$ ) which in our approach limits  $\sigma_w^2$ .